Semiconductor Physics, Quantum Electronics & Optoelectronics, 2015. V. 18, N 1. P. 40-45.
doi: 10.15407/ spqeo18.01.040

PACS 07.57.Kp, 73.40.-c, 85.30.Tv

Sub-THz nonresonant detection in AlGaN/GaN heterojunction FETs

A.G. Golenkov[1], K.S. Zhuravlev[2], J.V. Gumenjuk-Sichevska[1], I.O. Lysiuk[1], F.F. Sizov[1]
[1]V. Lashkaryov Institute of Semiconductor Physics, NAS of Ukraine,
41, prospect Nauky, 03028 Kyiv, Ukraine
E-mail: golenkov.o@gmail.com; gumenjuk@gmail.com; Lysiuk@gmail.com; sizov@isp.kiev.ua
[2]A. Rzhanov Institute of Semiconductor Physics, Siberian Branch of RAS,
13, pr. Lavrentieva, Novosibirsk, 630090 Russia; e-mail: zhur@thermo.isp.nsc.ru

Abstract. Un-cooled AlGaN/GaN-based heterojunction field-effect transistors (HFET) designed on sapphire (0001) substrates were considered as 140 GHz direct detection detectors without any specially attached antennas. The noise equivalent power (*NEP*) of these detectors was $\sim 10^{-10}\,\mathrm{W/Hz^{1/2}}$ in the observed radiation frequency range at ambient temperatures. It has been shown that the ultimate value for the AlGaN/GaN HFET detectors (in 0.25-μm technology) can reach $NEP_{\mathrm{opt}} \approx 6\cdot 10^{-12}\,\mathrm{W/Hz^{1/2}}$, and it is 3-fold lower than that for Si MOSFET (in 0.35-μm technology).

Keywords: sub-THz detectors, heterojunction FET, AlGaN/GaN heterostructure, Si MOSFET, sensitivity.

Manuscript received 06.10.14; revised version received 10.12.14; accepted for publication 19.02.15; published online 26.02.15.

1. Introduction

Terahertz (THz) technologies for radiation frequencies loosely defined from $\nu \sim 0.1$ to 10 THz [1, 2] ($\lambda \sim$ 3 mm…30 μm) are now the emerging ones, which promises wide choice for potential applications in vision systems, high speed wireless communications, spectroscopy, medicine, security, pharmacology, etc. [3, 4]. They can give relatively high resolution images. At the same time, the THz radiation is innocuous as it is not ionizing, e.g. for the human body in the case of active imaging. Along with sources, important components of these technologies are detectors. Uncooled detectors implemented as an integrated array are required to obtain real time imaging in many applications.

AlGaN/GaN-based heterojunction field-effect transistors (HFETs) have been reported as one of the most promising devices for high-power and high-frequency applications due to material properties of nitride-based compounds such as wide band-gap, high breakdown voltage and high two-dimensional electron gas (2DEG) density (see e.g. [5-7]). In recent years, attention to AlGaN/GaN-based HFETs is attracted because of their high potential applicability as sub-THz/THz detectors [8-10].

2. Advantages of AlGaN/GaN HFETs

The advantages of AlGaN/GaN HFETs over Si MOSFETs are higher channel electron mobility μ_n (by the factor approximately 4) and lower gate material resistivity (by the factor close to 100). Both of these factors provide the lower detector resistance R_0 and, as a result, the lower thermal (Johnson) noise U_J, which is the

Semiconductor Physics, Quantum Electronics & Optoelectronics, 2015. V. 18, N 1. P. 40-45.
doi: 10.15407/ spqeo18.01.040

principal noise of these detectors at biases around zero. It can be explained using the equation $R_0 = L/(W \cdot \mu_n \cdot C'_{OX} \cdot n \cdot \varphi_t)$ [11] for Si MOSFETs where the resistance R_0 is in direct proportion to the channel length L, inversely to the channel width W and mobility μ_n. Parameters C'_{OX}, n, φ_t are the oxide capacity, the *I–V* characteristic slope in the sub-threshold region, the thermal potential, respectively. Usually, the length L is designed as small as manufacturing design rules allow. But the width W can be optimized. To decrease resistance R_0, the width W should be increased. At the same time, the width W can not be very wide, because the gate parasitic serial resistance R_S becomes large according to [7]:

$$R_S = r_0 + r_1/W + r_2 \cdot W/(3L), \tag{1}$$

where r_0 is the resistance of the contacts between metal and gate layers (~5 Ω), r_1 – transistor source resistivity, and r_2 – gate material resistivity. Due to the fact that AlGaN/GaN HFET gate has a Schottky barrier, its metallic gate resistivity r_2 is considerably smaller than the polysilicon gate resistivity of Si MOSFET (see Fig. 1a). Typically, the Si MOSFET r_1 and r_2 values are $r_1 \sim 400\ \Omega\cdot\mu$m, $r_2 \sim 40\ \Omega$ (according to the 0.35-μm technology design rules), and the AlGaN/GaN HFET value $r_2 < 0.1\ \Omega$. To avoid power losses, the value of R_S have to be considerably lower than the antenna radiation resistance R_{AR} (~100 Ω).

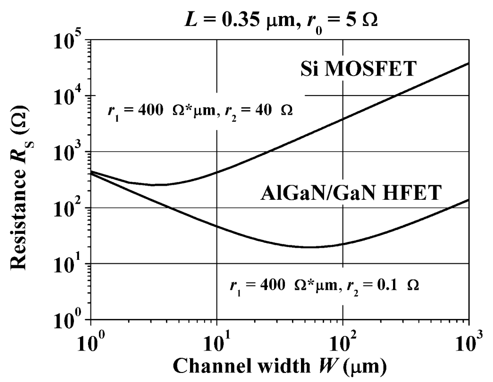

a

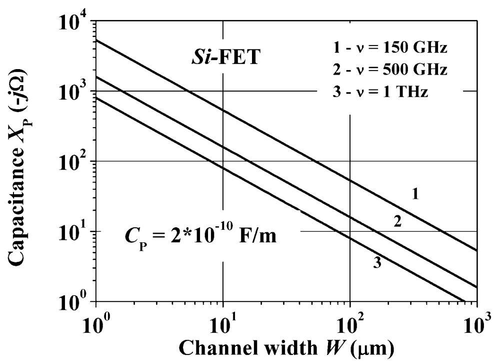

b

Fig. 1. Modeled channel width dependences of the parasitic serial resistance (*a*) and the shunting capacitance (*b*).

The width W limited also by parasitic shunting capacitance $X_P = -j/(2\pi\nu \cdot W \cdot C'_P)$ appeared between the transistor gate and the source [12] (ν is irradiation frequency), where C'_P is the shunting capacity density on the width unit (Fig. 1b). Value C'_P depends on the FET production technology (typically, the value $C'_P \approx 2 \cdot 10^{-10}$ F/m for 0.35-μm design rules).

It seems that the influence of the channel width W on capacitance X_P for AlGaN/GaN HFET and Si MOSFETs is the same.

3. Optical *NEP* and sensitivity of the rectifying type detectors

Sub-THz detectors based on zero-biased Schottky-barrier diodes (SBD) and field effect transistors (FET), heterojunction field effect transistors (HFET), high electron mobility transistors (HEMT) in low frequency (nonresonant) long gate regime [13] are detectors of rectifying type and can be described in a similar way [12].

Most of the previous publications (e.g. [14, 15]) concentrate their attention on the electrical noise equivalent power (*NEP*) rather than optical NEP_{opt}. The latter one takes into account antenna properties and its matching efficiency with detector. The optical NEP_{opt} and sensitivity $\Re_{\text{V,opt}}$ of the rectifying type detectors can be found from the modified equations adduced [12], according to which one can obtain the relatively simple analytical expressions for NEP_{opt} and sensitivity $\Re_{\text{V,opt}}$ are

$$NEP_{\text{opt}} = \frac{4 \cdot n \cdot q^{1/2} \cdot \varphi_t^{3/2} \cdot R_0^{1/2}}{R_{A,R}} \cdot \frac{f_\sigma^{1/2}}{F} \cdot \frac{1}{\xi_Z \cdot \xi_{\text{opt}} \cdot e_{cd} \cdot D_0}, \tag{2}$$

$$\Re_{V,\text{opt}} = \frac{R_{AR}}{2 \cdot n \cdot \varphi_t} \cdot \frac{F}{f_\sigma} \cdot \eta_L \cdot \xi_Z \cdot \xi_{\text{opt}} \cdot e_{cd} \cdot D_0, \tag{3}$$

where n is the *I–V* characteristic slope in the sub-threshold region (FET, HFET, HEMT) or ideality factor for SBD, q, R_0, e_{cd}, D_0, $\varphi_t = k_B T/q$, k_B, T are the elementary electronic charge, detector resistance, antenna radiation efficiency, antenna directivity, thermal potential, Boltzmann constant, and temperature, respectively. The coefficient $\eta_L = |Z_L/(R_D + Z_L)|$ defines the voltage divider between detector resistance R_D and external load impedances Z_L; the coefficient ξ_Z describes sub-THz frequency voltage divider between antenna Z_A and detector Z_{int} wave impedances in compliance with equation $\xi_Z = \left|\frac{X_P \,||\, Z_{\text{int}}}{Z_A + R_S + X_P \,||\, Z_{\text{int}}}\right|^2$, the coefficient ξ_{opt} is equal to $\xi_{opt} = \lambda^2/(4\pi \cdot A_{opt})$ (λ is the irradiation wavelength, A_{opt} is the detector physical area).

For FET, HFET, and HEMT, the function f_σ characterizes dependence of the conductivity σ on the gate-source voltage V_{GS} is

$$f_\sigma(x) = 2\cdot\exp(x/2)\cdot\ln[1+\exp(x/2)]/[1+\exp(x/2)],$$

where $x = (V_{GS} - V_{\rm th})/(n\cdot\varphi_t)$, $V_{\rm th}$ is the threshold voltages of the transistor. The function F is $F(x) = (2-n)\cdot(df_\sigma/dx)$, and the formula for internal impedance $Z_{\rm int}$ is $Z_{\rm int} = (1-j)\sqrt{R_0/(4\pi\nu\cdot W\cdot L\cdot C'_{OX})}\Big/ f_\sigma^{1/2}$ [12].

For zero-biased SBD detectors $f_\sigma(0) = F(0) = 1$.

The minimum value of the function $f_\sigma^{1/2}\cdot(df_\sigma/dx)^{-1} \approx 1.75$ and the maximum value of the function $(1/f_\sigma)\cdot(df_\sigma/dx) = 1$ (Fig. 2) define optimum $NEP_{\rm opt}$ and sensitivity $\Re_{V,\rm opt}$.

Using the expressions (1), (2) and assumptions $\eta_L = \xi_Z = \xi_{\rm opt} = D_0 = e_{cd} = 1$, one can estimate the ultimate performance values $NEP_{\rm opt}$ and sensitivity $\Re_{V,\rm opt}$ of rectifying type detectors as

$$\Re_{V,opt} \approx 1500\,\frac{\rm V}{\rm W}\cdot\left(\frac{1.3}{n}\right)\cdot\left(\frac{R_{AR}}{100}\right)\cdot\left(\frac{300}{T}\right)\cdot\frac{F}{f_\sigma}, \qquad (4)$$

$$NEP_{\rm opt} \approx 2.6\cdot10^{-12}\,\frac{\rm W}{\rm Hz^{1/2}}\cdot\frac{n}{1.3}\cdot\frac{100}{R_{AR}}\times \times\left(\frac{T}{300}\right)^{3/2}\cdot\left(\frac{R_0}{1000}\right)^{1/2}\cdot\frac{f_\sigma^{1/2}}{F}. \qquad (5)$$

Taking into account the optimum values of the functions $f_\sigma^{1/2}/F$ and F/f_σ are $\sim 1.75/(2-n)$ and $2-n$, respectively, from (3) and (4) at $n = 1.3$, $R_{AR} = 100\ \Omega$, $R_0 = 1000\ \Omega$ (for acceptable channel width in the 0.25-μm technology), and $T = 300$ K, we estimate the ultimate optical of the AlGaN/GaN HFET as $NEP_{\rm opt} \approx 6.5\cdot10^{-12}\ {\rm W/Hz^{1/2}}$ and sensitivity as $\Re_{V,\rm opt} \approx 1000$ V/W.

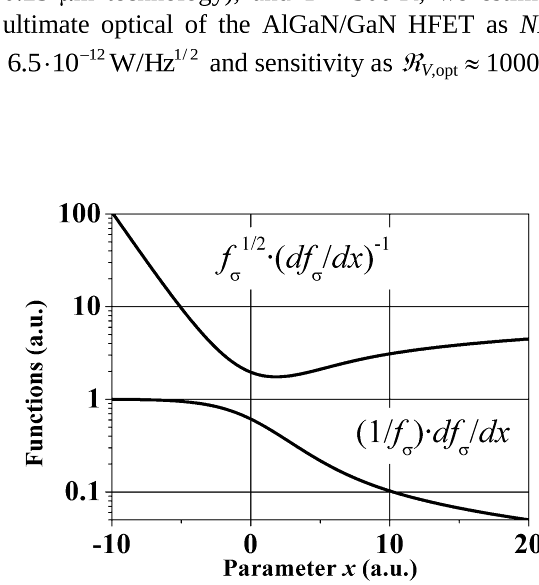

Fig. 2. Functions to calculate $NEP_{\rm opt}$ and sensitivity $\Re_{V,\rm opt}$.

In comparison with AlGaN/GaN HFET, the ultimate optical $NEP_{\rm opt}$ of Si MOSFETs will be worse by the factor ~3 because its minimal resistance $R_0 \sim 7.4$ kΩ (for an acceptable channel width in the 0.35-μm technology): for Si MOSFETs is equal to $NEP_{\rm opt} \approx 1.8\cdot10^{-11}\ {\rm W/Hz^{1/2}}$.

4. Samples

SBD and silicon field effect transistors are rather widely tested as sub-THz/THz uncooled detectors [2]. Here, to test heterostructure field effect transistors as sub-THz/THz detectors, commercial AlGaN/GaN HFETs were chosen.

The AlGaN/GaN heterostructures were grown on sapphire (0001) substrate of d = 400 μm thickness by molecular beam epitaxy method (MBE) using CBE RIBER 32 equipment at the temperature $T \sim 900$ °C. The cross section of the heterostructure is shown schematically in Fig. 3. The room temperature sheet electron concentration in the two-dimensional (2D) channel layer is $n_{300K} \approx 1.2\cdot10^{13}\ {\rm cm^{-2}}$, and the mobility is $\mu_{300K} \approx 1.46\cdot10^3\ {\rm cm^2/V\cdot s}$. They were measured using the Van der Pauw method in the magnetic field H = 0.5 T.

To decrease the substrate influence of detector response on radiation frequency and antenna gain, the Al_2O_3 substrates were polished to the thickness d = 175 μm. Here, the contact wires to HFETs pads serve as antennas. At this substrate thickness, the optical thickness $d\times(\varepsilon \approx 9.3)^{1/2} \approx 0.53$ mm (ε is the dielectric permittivity), which is less than the radiation wavelength in air λ = 2.14 mm, and though it does not satisfy the inequality $d(\varepsilon \approx 9.3)^{1/2} < 0.1$ mm to suppress the resonances in the substrate still it is making the response not strongly dependent on the radiation frequency

As for sub-THz detectors, sapphire substrate is not very appropriate, as its dielectric permittivity is high (perpendicular to c axis $\varepsilon_\perp \approx 9.3$, and parallel to c axes $\varepsilon_{||} \approx 11.5$), which leads to the large optical thickness and appearance of radiation modes within the substrate making the response dependent on the radiation frequency [16]. To exclude the influence of the substrate on frequency dependence of the registered signal, the estimations have shown the thickness of sapphire substrate d should not exceed $d = 0.25\lambda/\varepsilon^{1/2} \approx$ 150-175 μm for the radiation frequency 140 GHz and, for example, twice less for 300 GHz. To decrease the substrate influence of detector response on radiation frequency, the Al_2O_3 substrates were back thinned to the thickness d = 175 μm. Besides the suppression of the resonance modes in the substrate, and improving the antenna gain, it makes the system less sensitive to changing the frequency of radiation [17].

Shown in Fig. 4 is the linear array of five separate AlGaN/GaN HFETs detectors. Here, the contact wires to HFETs contact pads serve as antennas. We measured the photo-responses V_{sig} of these detectors on the frequency ν = 140 GHz at the ambient temperature. The sensitivities $\Re_V$ [V/W] were calculated.

At the threshold gate-source value $V_{th} \approx -4.3$ *V* of the studied transistors the channel resistance $R_{ch} \approx 200\ \Omega$ (ratio $L/W \approx 2.5 \cdot 10^{-3}$, width $W = 100$ μm).

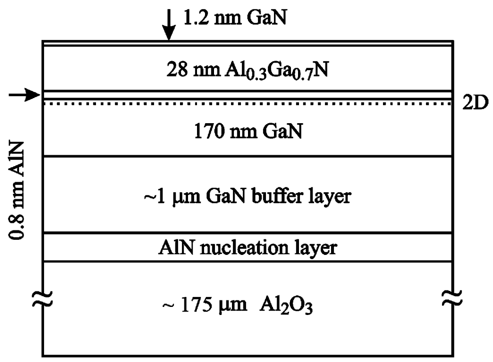

Fig. 3. The schematic cross-section of the AlGaN/GaN heterostructure.

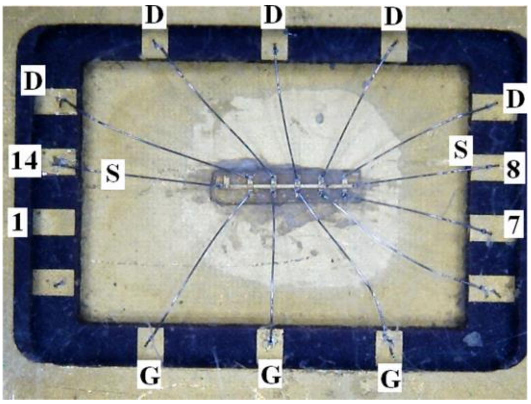

Fig. 4. The general view of five elements AlGaN/GaN HFET.

5. Results of the measurements

The noise equivalent power *NEP* is one of the most important parameters that characterizes detector. It determined as $NEP = V_{noise} / \Re_V$ (W/Hz$^{1/2}$), where V_{noise} is the detector noise voltage, and the voltage sensitivity $\Re_V = V_{sig}/P_{THz}$, P_{THz} is the radiation power falling down onto detector.

To estimate the detector sensitivity, the relative power distribution from the 140 GHz source was mapped using the sub-THz/THz detector at sample displacement. Experimental points satisfy well the Fraunhofer diffraction intensity dependence with the Airy disk diameter $\approx 2.44 \cdot \lambda_0 \cdot F/\# \approx$ 13 mm (for optical system *f*-number $F/\# \approx 2.5$). Concentrated in the Airy disk is approximately 84% of radiation power from the source, reflection and absorption losses of optical system were estimated as 70%, and the absolute power from the source was $P \approx 15$ mW. The power at the detector in its centre was calculated according to the method presented in [18] using the Gauss function that fits well the power distribution. The radiation power density $I_{THz} \approx 0.071$ W/cm^2 at the sample displacement according to these calculations. Note that the maximum possible antenna effective area $A_{eff} = G \cdot \lambda^2 / (4\pi) \approx 0.36$ mm^2 [19] (here, the antenna gain *G* was taken as *G* = 1).

For FET THz detectors, the main noise V_{noise} in the zero-bias regime is the thermal one [14]. It was calculated from the equation $V_{noise} = \sqrt{4 \cdot k_B \cdot T \cdot R_{ch}}$ where dependence of the channel resistance R_{ch} on the gate-source voltage V_{GS} was measured. These values were used for *NEP* estimations. The calculated thermal noise is shown in Fig. 5. Due to the intrinsic noise of the lock-in amplifier (Stanford SR 830) used to detect, the signal is not less than 6 nV/Hz$^{1/2}$, the lowest detector noise cannot be measured. The minimal $NEP \approx 10^{-10}$ W/Hz$^{1/2}$ is observed at the gate-source voltage V_{GS} = - 4.6 V (Fig. 5).

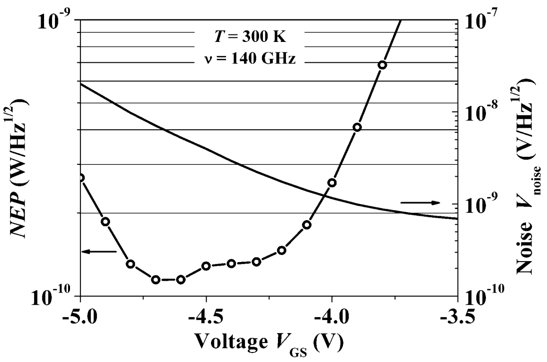

Fig. 5. The *NEP* and calculated thermal noise dependences on the gate-source voltage for AlGaN/GaN HFET.

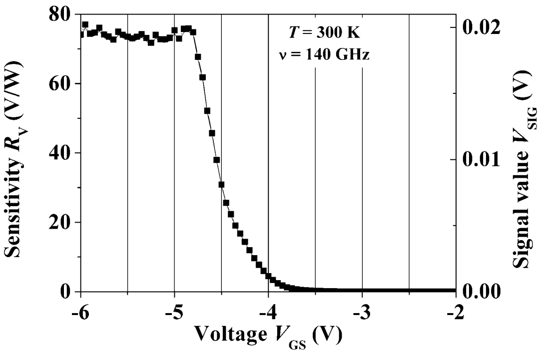

Fig. 6. The signal V_{sig} and corresponded sensitivity $\Re_V$ dependences on the gate-source voltage for AlGaN/GaN HFET.

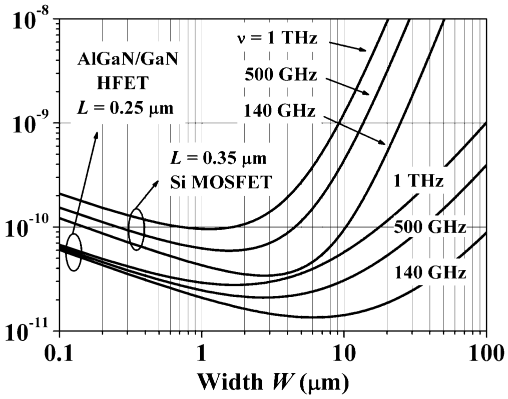

Fig. 7. Calculated using the equation (2) *NEP* dependences on the width *W* of the transistors for AlGaN/GaN HFET (0.25-μm design rules) and Si MOSFET (0.35-μm design rules) at various irradiation frequencies.

The signal V_{sig} dependence for one of HFET on the gate-source voltage is shown in Fig. 6. One can see saturation of this dependence [20] at high values of V_{GS} (left part of Fig. 6). It is conditioned with the equations for signal $V_{sig} \sim (\sigma_{ch})^{-1} \cdot (d\sigma_{ch}/dV_{GS})$ and the channel conductivity $\sigma_{ch} = \sigma_0 \cdot \exp[(V_{GS} - V_{th})/(nk_B T)]$ in the sub-threshold region, σ_0 is the channel conductivity at threshold value. The sensitivity $\Re_V$ dependence on V_{GS} used for *NEP* estimations is shown in Fig. 6. These values of sensitivity $\Re_V$ together with relatively low noise level of AlGaN/GaN HFET can provide the values of *NEP* which are comparable with those for other uncooled detectors [2].

6. Discussion

The experimentally measured value $NEP \approx 10^{-10}\,\mathrm{W/Hz^{1/2}}$ is less than its ultimate value by the factor of 10, and it agrees with the results of calculations presented in Fig. 7. The optimal channel width W_0 at the irradiation frequency 140 GHz is 6 μm ($NEP \approx 1.35 \cdot 10^{-11}\,\mathrm{W/Hz^{1/2}}$). But the width of investigated (commercial) samples was 100 μm (very high shunting capacitance). Mathematically, it is defined by the coefficient ξ_Z: $\xi_Z = 0.54$ ($W = 6$ μm), and $\xi_Z = 0.02$ ($W = 100$ μm).

To calculate the dependences (Fig. 7), we used the following parameters for AlGaN/GaN HFET $L = 0.25$ μm, $C'_{OX} \approx 2.73 \cdot 10^{-3}\,\mathrm{F/m^2}$, $C'_P \approx 1.23 \cdot 10^{-10}\,\mathrm{F/m}$, $n = 1.3$, $x = 3$, $\mu_n = 1500\ \mathrm{cm^2/V \cdot s}$, $Z_A = 100 - 100j$, $r_0 = 5\ \Omega$, $r_1 = 400\ \Omega \cdot \mu m$, $r_2 = 0.1\ \Omega$, $\xi_{opt} = e_{cd} = D_0 = 1$, and for Si MOSFET $L = 0.35$ μm, $C'_{OX} \approx 4.5 \cdot 10^{-3}\,\mathrm{F/m^2}$, $C'_P = 2 \cdot 10^{-10}\,\mathrm{F/m}$, $n = 5$, $x = 3$, $\mu_n = 400\ \mathrm{cm^2/V \cdot s}$, $Z_A = 100 - 100j$, $r_0 = 5\ \Omega$, $r_1 = 400\ \Omega \cdot \mu m$, $r_2 = 40\ \Omega$, $\xi_{opt} = e_{cd} = D_0 = 1$.

The values of *NEP* presented in [21] for InGaAs FETs ($NEP \sim 8 \cdot 10^{-12}\,\mathrm{W/Hz^{1/2}}$) seems as overestimated ones as for V_{sig} and *NEP* calculations the effective antenna area was taken a physical area of the structure with the chain of four FETs only (without area of the contacts), which is several times lower than the effective area of the antenna $\lambda^2/4\pi$ [16, 19] that was taken in this article as a normalization constant.

7. Conclusions

Nonresonant detection of the sub-THz radiation in AlGaN/GaN HFETs has been investigated. It has been shown the main its advantages in comparison with Si MOSFETs are higher channel electron mobility and lower gate material resistivity (metallic one in contrast to polysilicon in Si MOSFETs). As a result, the resistance, thermal noise, and noise equivalent power of the AlGaN/GaN HFET detectors are less than their values in Si MOSFETs one by factors of ~10, ~3, and ~3, respectively.

Equations for optical voltage sensitivity $\Re_{V,\mathrm{opt}}$ and optical NEP_{opt} allow calculation of their ultimate values for the AlGaN/GaN HFET detectors, which are equal to $\Re_{V,\mathrm{opt}} \approx 1000$ V/W and $NEP_{\mathrm{opt}} \approx 6.5 \cdot 10^{-12}\,\mathrm{W/Hz^{1/2}}$, respectively, at room temperatures for 0.25-μm technology design rules.

The values of sensitivity $\Re_{V,\mathrm{opt}} \sim 80$ V/W and noise equivalent power $NEP_{\mathrm{opt}} \sim 10^{-10}\,\mathrm{W/Hz^{1/2}}$ obtained in the samples investigated are sufficiently worse as compared to their estimated ultimate values and can be explained by lack of the special designed receiving antennas to the detectors and large transistor width though these values are typical for other uncooled THz/sub-THz detectors.

The optimal width of the transistors depends on irradiation frequency and technology design rules. For AlGaN/GaN HFET detectors manufactured using 0.25-μm technology, the optimal width W_0 is equal to 6, 2.7, and 1.6 μm for frequencies 140 GHz, 500 GHz, and 1 THz, respectively.

Acknowledgement

Authors are very thankful to Research Fellow Svetlana G. Bunchuk for her scrupulous attitude towards preparation of the samples, and Dr. Mikolay V. Sakhno for useful discussions.

This work was partly supported by Ukrainian Program of Basic Researches (grant No. 11/14-H) and joint project of Ukrainian National Academy of Sciences (grant No. 01-02-2012) and Siberian Branch of Russian Academy of Sciences (grant No. 15.1).

References

1. A.G. Davies, A.D. Burnett, W.H. Fan, E.H. Linfield and J.E. Cunningham, Terahertz spectroscopy of explosives and drugs // *Materials Today*, **11**(3), p. 18-26 (2008).

2. F. Sizov, A. Rogalski, THz detectors // *Progr. Quant. Electr*. **34**(5), p. 278-347 (2010).
3. R. Appleby, H.B. Wallace, Standoff detection of weapons and contraband in the 100 GHz to 1 THz region // *IEEE Trans*. *Antennas Propag*. **55**, p. 2944-2956, 2007.
4. Kai-Erik Peiponen, J. Axel Zeitler and Makoto Kuwata-Gonokami (eds.), *Terahertz Spectroscopy and Imaging*. Springer Series in Optical Sciences, **171**, Heidelberg–New York–Dordrecht–London, 2013, p. 1-641.
5. Y.C. Choi, J. Shi, M. Pophristic, M.G. Spencer, and L.F. Eastman, C-doped semi-insulating GaN HFETs on sapphire substrates with a high breakdown voltage and low specific on-resistance // *J. Vac. Sci. Technol. B*, **25**, p. 1836-1841 (2007).
6. M. Kuroda, H. Ishida, T. Ueda, and T. Tanaka, Nonpolar (11-20) plane AlGaN/GaN heterojunction field effect transistors on (1-102) plane sapphire // *J. Appl. Phys*. **102**, Article ID 093703, 2007, p. 1-8.
7. M.S Shur and P. Maki (eds.), Advanced High Speed Devices, in: *Selected Topics in Electronics and Systems*, **51**, World Scientific, Singapore, 2009, p. 1-187.
8. El Fatimy, S.B. Tombet, F. Teppe, W. Knap, D.B. Veksler, S. Rumyantsev, M. Shur, Terahertz detection by GaN/AlGaN transistors // *Electron. Lett.* **42**, p. 1342-1343 (2006).
9. L. Liu, B. Sensale-Rodriguez, Z. Zhang, T. Zimmermann, Y. Cao, D. Jena, P. Fay, and H. Xing, Development of microwave and terahertz detectors utilizing AlN/GaN high electron mobility transistors // *Proc. 21st ISSTT*, Oxford, 2010, p. 321-325.
10. P. Sangare, G. Ducournau, B. Grimbert et al., Experimental demonstration of direct terahertz detection at room-temperature in AlGaN/GaN asymmetric nanostructures // *J. Appl. Phys.* **113**, Article ID 034305, p. 1-6 (Jan. 2013).
11. Y. Tsividis, C. McAndrew, *Operation and Modeling of the MOS Transistor*, 3rd ed. Oxford University Press, New York, 2011, p. 1-726.
12. M. Sakhno, A. Golenkov, and F. Sizov, Uncooled detector challenges: Millimeter-wave and terahertz long channel field effect transistor and Schottky barrier diode detectors // *J. Appl. Phys.* **114**, 164503 (2013).
13. W. Knap, M. Dyakonov, D. Coquillat et al., Field Effect Transistors for Terahertz Detection: Physics and First Imaging Applications // *J. IRMMW-THz*, **30**, p. 1319-1337 (Dec. 2009).
14. R. Tauk, F. Teppe, S. Boubanga et al., Plasma wave detection of terahertz radiation by silicon field effects transistors: Responsivity and noise equivalent power // *Appl. Phys. Lett.* **89**, Article ID 253511, p. 1-3 (Dec. 2006).
15. E. Ojefors, U.R. Pfeiffer, A. Lisauskas, H.G. Roskos, A 0.65 THz focal-plane array in a quarter-micron CMOS process technology // *IEEE J. Solid-State Circuits*, **44**, p. 1968-1976 (2009).
16. *Antenna Engineering Handbook*, 4th ed., J.L. Volakis (ed.). McGraw-Hill Companies, New York, 2007, p. 1-1755.
17. M. Sakhno, J. Gumenjuk-Sichevska and F. Sizov, Modeling of the substrate influence on multi-element THz detector operation // *J. IRMMW-THz*, **35**, p. 703-719 (2014).
18. F. Sizov, V. Petriakov, V. Zabudsky, D. Krasilnikov, M. Smoliy, and S. Dvoretski, Millimeter-wave hybrid un-cooled narrow-gap hot-carrier and Schottky diodes direct detectors // *Appl. Phys. Lett*. **101**, 082108 (2012).
19. C.A. Balanis, *Antenna Theory: Analysis and Design*. 3rd ed., Wiley-Interscience, A John Wiley & Sons, Inc., 2005, p. 1-1072.
20. M. Sakowicz, M.B. Lifshits, O.A. Klimenko, F. Schuster, D. Coquillat, F. Teppe, and W. Knap, Terahertz responsivity of field effect transistors versus their static channel conductivity and loading effects // *J. Appl. Phys.* **110**, Article ID 054512, p. 1-6 (Sep. 2011).
21. V.V. Popov, D.M. Yermolaev, K.V. Maremyanin et al., Detection of terahertz radiation by tightly concatenated InGaAs field-effect transistors integrated on a single chip // *Appl. Phys. Lett*. **104**, Article ID 163508, p. 1-4 (2014).